Dipole strength in 80Se for s process and nuclear transmutation of 79Se

Makinaga, A.; Massarczyk, R.; Beard, M.; Schwengner, R.; Otsu, H.; Al-Abdullah, T.; Anders, M.; Bemmerer, D.; Hannaske, R.; John, R.; Junghans, A. R.; Müller, S. E.; Röder, M.; Schmidt, K.; Wagner, A.;

Dipole strength in ^{80}Se for s process and nuclear transmutation of ^{79}Se

A. Makinaga,[1, 2, *] R. Massarczyk,[3, †] M. Beard,[4] R. Schwengner,[3] H. Otsu,[5] T. Al-Abdullah,[6] M. Anders,[3]
D. Bemmerer,[3] R. Hannaske,[3] R. John,[3] A. R. Junghans,[3] S. E. Müller,[3] M. Röder,[3] K. Schmidt,[3, 7, ‡] and A. Wagner[3]

[1]*Faculty of Science, Hokkaido University, Kita-15, Nishi-7, Kita-ku, 060-8638 Sapporo, Japan*
[2]*JEIN Institute for Fundamental Science, 5-14, Yoshida-Honmachiu, Sakyo-ku, 606-8317 Kyoto, Japan*
[3]*Helmholtz-Zentrum Dresden-Rossendorf, 01328 Dresden, Germany*
[4]*Department of Physics, University of Notre Dame, Notre Dame, Indiana 46556, USA*
[5]*RIKEN Nishina Center, 2-1 Hirosawa, Wako, Saitama 351-0198, Japan*
[6]*Hashemite University, Zarqa, Jordan*
[7]*Technische Universität Dresden, 01062 Dresden, Germany*
(Dated: June 20, 2016)

The dipole strength distribution of ^{80}Se was studied in a photon-scattering experiment using bremsstrahlung produced with an electron beam of energy 11.5 MeV at the linear accelerator ELBE. We identified 180 γ transitions up to an energy of 9.6 MeV, and analyzed the strength in the quasicontinuum of the spectrum. Simulations of statistical γ-ray cascades were performed to estimate intensities of inelastic transitions, and to correct the intensities of the ground-state transitions for their branching ratios. The photoabsorption cross section below the neutron-separation energy derived in this way was combined with the photoabsorption cross section obtained from an earlier (γ, n) experiment and used as an input for the calculation of ^{79}Se(n, γ) reaction rates on the basis of the statistical reaction model.

I. INTRODUCTION

The γ-ray strength function (γSF) is an important ingredient for the estimate of cross sections of photonuclear reactions and their inverse reactions in not only nuclear physics, but also for nuclear applications such as nuclear medicine and nuclear engineering. In the past half century, the giant dipole resonance (GDR) has been investigated both experimentally and theoretically via photo-nuclear reactions by many researchers[1, 2]. Nowadays, more precise measurements of photo-neutron reactions near the neutron threshold (S_n) are performed by using quasi-monochromatic γ rays [3–6]. The low-energy tail of the GDR below S_n is of particular interest because of an extra enhancement of observed $E1$ strength. This pygmy dipole resonance (PDR) [7–9], has been found e.g. in ^{76}Se [10], ^{78}Se [11], nuclides with $Z = 42$ [12, 13], $N = 50$ [14–18], nuclides around $N = 82$ [19–28], in ^{181}Ta [29], and in the doubly magic ^{208}Pb [30–32].

From the nuclear-astrophysics point of view, approximately half of the elements heavier than iron are synthesized in the stellar environment by the slow neutron-capture process (s-process), which synthesizes nuclei on the valley of β stability (see Ref. [34] and Refs. therein). Classically, the s-process is divided into two components,

namely a weak and a main component [34]. The weak s-process ($A < 90$) is considered to proceed via the core He-burning and shell C-burning phase. The reaction ^{22}Ne$(\alpha,n)^{25}$Mg is the main neutron source in massive stars ($M \sim 25M_\odot$). The weak component proceeds at neutron densities of $n_n = 10^6 - 10^7$ cm^{-3} and temperatures of $T \sim 3 \cdot 10^8$ K [35]. The main s-process component ($A > 90$) is believed to take place in the asymptotic giant branch (AGB) stage of low-mass stars ($M < 8M_\odot$) [33, 36]. In this case, one of the neutron sources is the ^{13}C$(\alpha, n)^{16}$O reaction in the ^{13}C pocket after a convective He-shell flash ($T \sim 10^8$ K and $n_n \sim 7 \cdot 10^7$ cm^{-3}) contributing to the s-process for a long duration of 20,000 a. Another possible neutron source, ^{22}Ne$(\alpha,n)^{25}$Mg, also produces s-process elements in the He-flash region ($T \sim 2.7 \cdot 10^8$ K and $n_n \sim 10^{10}$ cm^{-3}) for a few years [37–43].

The s-process flow includes branching points when neutron capture and β decay compete. Because the neutron capture rate and β-decay rates have unique temperature dependencies, branching points can be used both as a stellar thermometer and a neutron density meter to estimate the s-process environment. Analyses of s-process branchings have already been attempted in other works [35, 47–51]. For the weak s-process component, one important branching point relates to ^{79}Se [50, 53–55]. The ground state of ^{79}Se has a long half-life of $T_{1/2} = 295,000$ a [56]. In addition, at 95.7 keV ^{79}Se has an isomer with $\log_{ft} = 4.70^{+0.10}_{-0.09}$ [47]. The isomer is thermally populated in the s-process environment and, because of the large β-decay probability, the effective β-decay rate is enhanced. The half-lives of the β^--decay branch points ^{79}Se and ^{80}Br, lead to the production of the s-only nucleus ^{80}Kr. On the other hand, the neutron capture branch at ^{79}Se, together with a minor branch of EC$^+$,

*Present address: Graduate school of Medicine, Hokkaido University, Kita-15, Nishi-7, Kita-ku, 060-8638 Sapporo, Japan
†Present address: Los Alamos National Laboratory, Los Alamos, New Mexico 87545, USA
‡Present address: National Superconducting Cyclotron Laboratory, Michigan State University, East Lansing, Michigan 48824, USA

β^+ decay at ^{80}Br, lead to the production of another s-only nucleus: ^{82}Kr. Therefore, the abundance ratio of ^{80}Kr/^{82}Kr, combined with related reaction rates, can provide information about temperature and neutron density in the s-process nucleosynthesis.

In the present stage, stellar β-decay rates for nuclei thermally equilibrated in stars are difficult to determine in the laboratory compared with terrestrial rates for nuclei in the ground states. More crucial is that it is impossible to measure neutron-capture cross sections for radioactive nuclei in the laboratory.

From the viewpoint of nuclear engineering, the radiative capture cross section of ^{79}Se is important for the development of transmutation techniques for long-lived fission products (LLFPs). The long-lived isotope ^{79}Se is a fission product and a component of spent nuclear fuel. It is chemically volatile and has the potential to migrate the biosphere from a deep geological disposal facility on time scales of 10^5 years [57]. Currently, the direct measurement of the neutron-capture cross section with a radioactive sample of ^{79}Se is proposed at the n-TOF facility of CERN [58]. In this case, ^{79}Se can be obtained by using the thermal neutron-capture reaction of a ^{78}Se - ^{208}Pb sample. In J-PARC, the neutron-capture cross section for ^{79}Se was evaluated on the basis of systematic measurements of neutron-capture cross sections for other Se isotopes [59, 60]. Recently, an experiment at the RIBF facility at RIKEN also aimed at the determination of the radiative-capture cross section of ^{79}Se by using a ^{79}Se beam in inverse kinematics [61]. Stable ^{80}Se, which is obtained from neutron capture on ^{79}Se, shows potential also as photoelectric device and pharmaceutical product.

Photodisintegration, which is a good probe of the $E1$ γ strength function (γSF), can be used to predict the "inverse" neutron capture cross sections for radioactive nuclei. Attempts to derive the ^{79}Se(n,γ)^{80}Se cross section using the γSF method have already been performed using Laser Compton backscattering (LCS) γ rays [62–64]. However, uncertainties of the γSF below the neutron-separation energy still remain.

The present work describes a study of the dipole strength of ^{80}Se using the (γ, γ') reaction at the bremsstrahlung facility γELBE [65] at the Helmholtz-Zentrum Dresden-Rossendorf. Photon scattering from nuclei, also called nuclear resonance fluorescence (NRF), is a suitable tool to study dipole strength functions below S_n. Predominantly states with spin $J = 1$ and, to a lesser extent, states with $J = 2$ are excited from the ground state in an even-even nucleus. NRF experiments aim at the determination of the photoabsorption cross section σ_γ and the dipole strength function f_1 on an absolute scale. In photoexcitation, the two quantities are connected via the relation $f_1 = \sigma_\gamma/[g(\pi\hbar c)^2 E_\gamma]$ with $g = (2J_x + 1)/(2J_0 + 1)$, where J_0 and J_x are the spins of the ground state and the excited state, respectively.

In earlier NRF studies of ^{80}Se, the deexcitation of a level at 7820 keV was investigated [66, 67]. In the present work, we identified 180 γ rays up to 9.6 MeV in ^{80}Se, but

a 7820 keV γ ray was not among them. We determined the photon-scattering cross section in 10 keV bins of excitation energy, up to $S_n = 9.9$ MeV. In this analysis, the intensity in the quasicontinuum part of the spectrum was taken into account. Moreover, we estimated intensities of inelastic transitions to low-lying excited states and average branching ratios of the ground-state transitions by means of simulations of statistical γ-ray cascades. Using these quantities, we determined the photoabsorption cross section.

II. EXPERIMENTAL METHODS AND RESULTS

A. The photon-scattering method

In photon-scattering experiments, the energy- and solid-angle-integrated scattering cross section I_s of an excited state at an energy E_x, can be deduced from the measured intensity of the respective transition to the ground state. It can be determined relative to known integrated scattering cross sections. In the present experiments, we used the integrated scattering cross sections $I_s(E_x^B)$ of states in ^{11}B [68] and their angular correlations including mixing ratios [69] as a reference:

$$\frac{I_s(E_x)}{I_s(E_x^B)} = \left(\frac{I_\gamma(E_\gamma, \theta)}{W(E_\gamma, \theta)\Phi_\gamma(E_x)N_N}\right)\left(\frac{I_\gamma(E_\gamma^B, \theta)}{W(E_\gamma^B, \theta)\Phi_\gamma(E_x^B)N_N^B}\right)^{-1}.$$
(1)

Here, $I_\gamma(E_\gamma, \theta)$ and $I_\gamma(E_\gamma^B, \theta)$ denote the measured intensities of a considered ground-state transition at E_γ and of a ground-state transition in ^{11}B at E_γ^B, respectively, observed at an angle θ to the beam. $W(E_\gamma, \theta)$ and $W(E_\gamma^B, \theta)$ describe the angular correlations of these transitions. The quantities N_N and N_N^B are the numbers of nuclei in the ^{80}Se and ^{11}B targets, respectively. The quantities $\Phi_\gamma(E_x)$ and $\Phi_\gamma(E_x^B)$ stand for the photon fluxes at the energy of the considered level and at the energy of a level in ^{11}B, respectively.

The integrated scattering cross section is related to the partial width of the ground-state transition Γ_0 according to

$$I_s = \int \sigma_{\gamma\gamma}\,dE = \left(\frac{\pi\hbar c}{E_x}\right)^2 \frac{2J_x + 1}{2J_0 + 1}\frac{\Gamma_0^2}{\Gamma},$$
(2)

where $\sigma_{\gamma\gamma}$ is the elastic scattering cross section, E_x, J_x and Γ denote energy, spin and total width of the excited level, respectively, and J_0 is the spin of the ground state.

The determination of the total level widths is complicated by two problems. First, a considered level can be fed by transitions from higher-lying states and second, a considered level can deexcite to low-lying excited states (inelastic scattering) in addition to the deexcitation to the ground state (elastic scattering). In the case of feeding, the measured intensity of the ground-state transition

is greater than the one resulting from a direct excitation only. As a consequence, the integrated scattering cross section I_{s+f} deduced from this intensity contains a portion I_f originating from feeding in addition to the true integrated scattering cross section I_s. In the case of inelastic scattering, inelastic and subsequent cascade transitions appear in the measured spectrum in addition to ground-state transitions. To deduce the partial width of a ground-state transition Γ_0 and the absorption cross section, one needs to know the branching ratio $b_0 = \Gamma_0/\Gamma$.

Spins of excited states can be deduced by comparing experimental ratios of intensities, measured at two angles, with theoretical predictions. The optimum combination comprises angles of 90° and 127° because the respective ratios for the spin sequences $0 - 1 - 0$ and $0 - 2 - 0$ differ most at these angles. The expected values are $W(90°)/W(127°)_{0-1-0} = 0.74$ and $W(90°)/W(127°)_{0-2-0} = 2.18$ taking into account opening angles of 16° and 14° of the detectors placed at 90° and 127°, respectively, in the setup at γELBE.

B. The target

The target consisted of 1952.9 mg selenium formed into a disk of 2 cm in diameter. The material was enriched to 99.9% ^{80}Se. The Se target was combined with 200.0 mg of ^{11}B, enriched to 99.5%, and also shaped into a disk of 2 cm diameter, to determine the photon flux from known scattering cross sections of levels in ^{11}B.

C. Detector response

To determine the integrated scattering cross sections according to Eq. (1), the relative efficiencies of the detectors and the relative photon flux were needed. The determination of the absorption cross section, described in Sec. II E, required correction to the experimental spectrum for detector response, absolute efficiency and absolute photon flux due to atomic processes, such as Compton scattering and pair creation induced by the impinging photons in the target material, and for ambient background radiation. The detector response was simulated using the program package GEANT4 [70]. The reliability of the simulation was tested by comparing simulated spectra with measured ones as described in Refs. [12, 14, 25].

The absolute efficiencies of the HPGe detectors in the setup at ELBE were determined experimentally up to 2.4 MeV from measurements with ^{137}Cs, ^{154}Eu, and ^{226}Ra calibration sources. For interpolation, an efficiency curve calculated with GEANT4 and scaled to the absolute experimental values was used. A check of the simulated efficiency curve up to about 9 MeV was performed via various (p,γ) reactions at the HZDR Tandetron accelerator. The efficiency values deduced from these measurements agreed with the simulated values within their uncertain-

ties [71]. Similar results were obtained for the resonances at 4.44 and 11.66 MeV in ^{12}C populated in the ^{11}B(p,γ) reaction at the TUNL van-de-Graaf accelerator [72].

D. Experiments with bremsstrahlung at γELBE

The nuclide ^{80}Se was studied at the bremsstrahlung facility γELBE. Bremsstrahlung was produced using an electron beam of kinetic energies of $E_e = 11.5$ MeV. The average current was about 710 μA. The electron beam hit a niobium foil of 7 μm thickness. A 10 cm thick aluminum absorber was placed behind the radiator to reduce the low-energy part of the bremsstrahlung spectrum (beam hardener). The photon beam, collimated by a 2.6 m long pure-aluminum collimator with a conical borehole of 8 mm diameter at the entrance and 24 mm diameter at the exit, impinged onto the target with a flux of about 10^9 s^{-1} in a spot of 38 mm diameter. Scattered photons were measured with three high-purity germanium (HPGe) detectors. Each had an efficiency of about 100% relative to a NaI detector of 7.6 cm diameter and 7.6 cm length. All HPGe detectors were surrounded by escape-suppression shields made of bismuth germanate (BGO) scintillation detectors of 3 cm thickness. The scintillation detectors were shielded against scattered photons by 10 cm thick lead blocks at the front and 3 cm thick lead casings around the sides. One HPGe detector was placed horizontally at 90° relative to the photon-beam direction and a distance of 28 cm from the target. The other two HPGe detectors were positioned in a vertical plane at 127° to the beam and a distance of 32 cm from the target. Absorbers of 8 mm Pb plus 3 mm Cu were placed in front of the detector at 90° and absorbers of 3 mm Pb plus 3 mm Cu were placed in front of the detectors at 127° to further reduce the count rate due to low-energy photons. Spectra of scattered photons were measured for 115 h. A spectrum including events measured with the two detectors placed at 127° relative to the beam at an electron energy of 11.5 MeV, is shown in Fig. 1.

The absolute photon flux at ELBE was determined from intensities and known integrated scattering cross sections of transitions in ^{11}B. For interpolation, the photon flux was calculated using a code [73] based on the approximation given in Ref. [74] and including a screening correction according to Ref. [75]. In addition, the flux was corrected for the attenuation by the beam hardener. This flux curve was adjusted to the experimental values obtained at the energies of levels in ^{11}B and is shown in Fig. 2.

For the transitions observed in the present measurement, we checked whether the sum of the energies of a considered transition and the first, second or third 2^+ states fit the energy of a higher-lying transition within the sum of the uncertainties. If this was the case, the transitions were considered as inelastic transitions and were sorted out. However, there may exist inelastic transitions with energy uncertainties larger than 0.3 keV, as
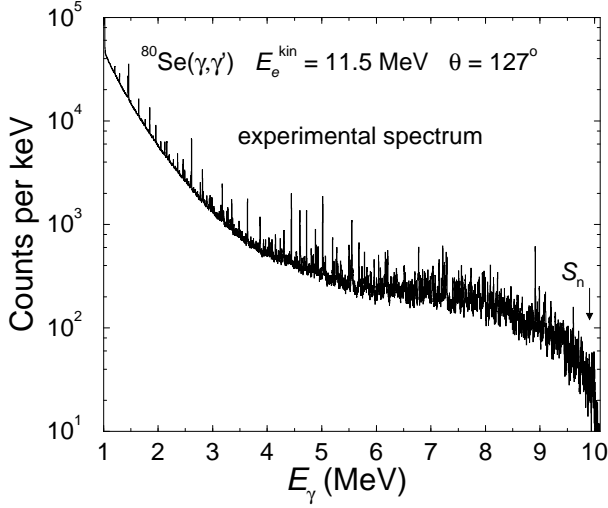
FIG. 1: (Color online) Spectrum of γ rays scattered from ^{80}Se combined with ^{11}B, measured during the irradiation with bremsstrahlung produced by electrons of an energy of $E_e^{\text{kin}} =$ 11.5 MeV. This spectrum is the sum of the spectra measured with the two detectors placed at $127°$ relative to the beam.
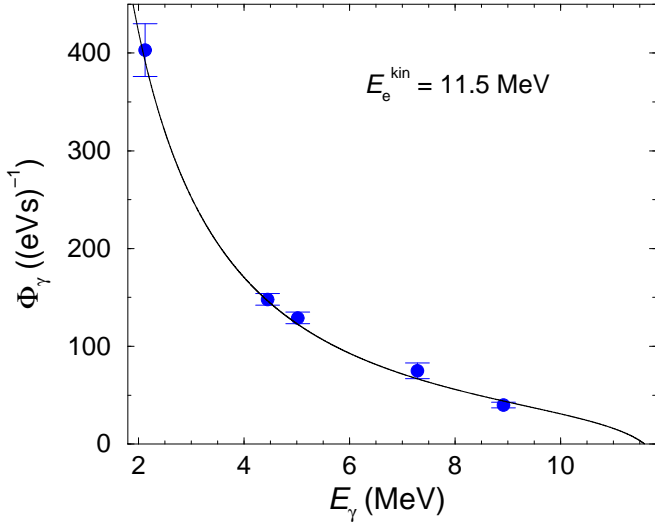

FIG. 2: (Color online) Absolute photon flux at the target deduced from intensities of four known transitions in ^{11}B (circles) using the detector efficiency calculated with GEANT4 and the relative flux calculated as described in the text (solid line).

well as transitions that feed low-lying levels other than the lowest three 2^+ states, and cascade transitions that depopulate those low-lying states to the ground state. Therefore, we list transition energies and angular correlations in Table I. Spins and integrated scattering cross sections are given under the assumption of ground-state transitions.

TABLE I: Gamma rays assigned to ^{80}Se.

E_γ(keV)[1]	$\frac{I_\gamma(90°)}{I_\gamma(127°)}$[2]	J_x^π[3]	I_s(eV b)[4]
666.3(2)		2^+[5]	
1449.4(2)		2^+[5]	
1646.2(1)	1.08(17)		86(8)
1848.7(1)	1.00(15)		115(10)
1959.8(2)		2^+[5]	
2051.5(2)	0.99(18)		23.0(25)
2204.5(3)	0.67(23)	1	12.6(20)
2281.8(2)	1.33(28)		14.4(19)
2321.0(4)			6.3(16)
2359.1(1)	1.06(18)		44(4)
2392.1(4)	1.9(8)		8.8(22)
2460.0(1)	0.98(16)		44(4)
2490.3(2)	1.4(5)		20.2(25)
2533.0(4)	0.9(4)		8.7(26)
2560.6(5)	0.7(5)		6.9(19)
2776.1(2)	1.03(19)		40(4)
2814.5(1)	1.03(16)		68(6)
2827.9(2)	0.90(21)		19.4(22)
2894.8(2)	1.3(4)		13.7(19)
2954.6(2)	1.3(4)		20.9(28)
2974.2(3)	1.1(3)		17.8(26)
2995.0(3)	1.3(3)		19.7(27)
3123.2(6)			11(3)
3177.0(1)	1.03(17)		64(6)
3193.0(3)	0.9(5)		12.0(20)
3262.5(2)	0.93(20)		18.2(20)
3279.9(2)	1.15(21)		25.1(26)
3299.0(4)	0.9(3)		7.8(13)
3329.5(3)	0.9(3)		11.6(19)
3350.5(1)	1.06(18)		43(4)
3443.6(9)	0.35(21)		14(8)
3506.0(4)	0.60(25)	1	8.1(21)
3538.0(6)			6.9(20)
3639.8(1)	0.78(13)	1	59(5)
3698.2(5)			5.3(15)
3795.5(6)	0.7(3)		6.9(20)
3820.1(15)			10(6)
3832.8(5)			5.2(16)
3869.8(2)	1.08(19)		37(4)
3932.6(3)			13.4(20)
3955.9(5)			7.8(17)
3993.2(9)			3.9(28)
4007.3(6)			7(4)
4033.1(3)	0.9(3)		14.7(25)
4044.6(5)			4.4(18)
4150.7(2)	0.99(21)		26.8(29)
4167.8(5)			7.6(15)
4239.6(3)	0.82(23)	(1)	15.4(21)
4293.6(8)			5.2(16)
4307.6(2)	0.91(16)	(1)	39(4)
4599.8(1)	0.76(12)	1	99(9)
4610.3(3)	1.02(19)		21.9(25)
4637.1(4)			9.5(26)
4687.2(4)	1.0(5)		12.0(20)
4722.1(1)	0.71(11)	1	100(9)
4806.4(2)	0.59(17)	1	29(4)
4820.4(8)			5.8(22)
4835.6(3)	0.9(3)		17.2(26)
4847.5(3)	0.9(3)		16.3(25)
4904.9(2)	0.72(22)	1	30(4)
4932.9(2)	0.58(13)	1	25.8(29)

5030.5(3)	0.81(21)	(1)	15.1(19)
5053.2(5)			9.9(21)
5067.2(3)	0.74(24)	1	18.8(25)
5199.4(2)	0.76(13)	1	62(6)
5225.7(4)	0.60(17)	1	24(4)
5263.9(3)	0.63(19)	1	22.0(28)
5275.9(2)	0.68(14)	1	40(4)
5343.7(4)	0.50(17)	1	16.8(26)
5350.2(4)	0.61(19)	1	14.7(23)
5371.2(20)			5.6(22)
5499.9(2)	0.94(23)		68(8)
5510.5(13)			12(4)
5536.4(3)	0.39(14)	1	21.6(25)
5551.1(1)	0.68(11)	1	115(10)
5681.7(2)	0.78(14)	1	55(5)
5737.0(3)	0.47(21)	1	31(5)
5783.2(2)	0.69(16)	1	36(4)
5800.5(6)			13(5)
5828.9(3)	0.64(26)	1	36(5)
5848.0(5)	1.1(5)		20(4)
5890.7(3)	0.42(15)	1	23(4)
5907.3(3)	0.56(16)	1	21(3)
5934.8(12)			22(12)
5960.3(3)	0.74(15)		44(5)
6002.5(5)	0.42(17)	1	18(5)
6041.5(2)	0.79(17)	1	35(4)
6073.0(3)	0.66(25)	1	31(4)
6093.3(7)			15(5)
6164.7(3)	0.72(17)	1	58(7)
6197.7(18)			15(5)
6209.0(3)	0.77(29)	(1)	75(10)
6232.2(7)			25(12)
6351.6(5)			20(4)
6368.1(6)			22(4)
6375.5(7)			18(3)
6496.9(6)			28(7)
6511.3(3)			57(8)
6526.4(4)			38(5)
6560.7(4)			15(4)
6604.2(7)			9.9(22)
6627.7(8)	0.18(5)	(1)	22(8)
6653.7(12)			23(6)
6673.3(6)			19(7)
6682.5(11)			14(9)
6705.4(4)	0.69(14)	1	27(5)
6721.8(13)			10(4)
6774.8(2)	0.65(11)	1	89(9)
6784.8(3)	0.63(15)	1	35(4)
6809.6(9)	0.20(6)	(1)	77(22)
6825.2(6)	0.40(20)	(1)	30(11)
6847.0(3)			28(5)
6879.1(3)	0.35(17)	(1)	34(10)
6891.4(4)	0.47(23)	(1)	27(8)
6944.1(3)	0.9(3)		20(3)
6966.0(7)			11(5)
6974.8(4)	1.0(3)		18(5)
6991.4(3)	0.52(20)	(1)	36(7)
7024.5(11)	0.69(25)	1	43(9)
7039.0(6)	0.60(15)	1	75(12)
7075.5(3)	0.77(23)	1	46(6)
7121.7(10)	0.46(24)	(1)	41(15)
7147.9(3)	0.66(16)	1	68(8)
7216.8(2)	0.80(18)	1	93(10)
7244.8(4)			54(12)
7261.1(4)			27(6)
7279.8(2)	0.71(13)	1	82(8)
7292.7(2)	0.59(11)	1	74(7)
7398.6(3)			23(4)
7430.8(4)			38(6)
7439.2(5)	0.56(26)	(1)	26(4)
7467.4(10)			24(7)
7483.2(5)			31(5)
7509.1(4)	1.2(3)		42(6)
7527.2(4)	1.1(4)		28(5)
7559.5(3)	0.60(13)	1	75(8)
7579.4(4)	0.56(13)	1	56(7)
7592.8(6)	0.47(17)	1	35(5)
7629.3(6)	0.49(15)	1	66(11)
7686.8(5)			33(6)
7717.7(5)	1.3(4)		28(4)
7746.3(6)	1.0(3)		22(4)
7805.3(5)			20(3)
7813.0(4)			23(3)
7857.2(6)	0.8(3)	(1)	36(6)
7864.6(10)			19(5)
7874.0(5)	0.66(29)	1	32(6)
7886.4(3)	0.7(3)	(1)	53(9)
7943.5(3)	0.57(22)	1	48(6)
7973.2(5)	0.82(23)	(1)	49(8)
7991.2(6)	0.7(3)	(1)	36(8)
8039.2(3)			28(4)
8071.9(5)			27(6)
8088.9(2)	1.24(23)		94(10)
8102.2(7)	1.8(6)		20(4)
8128.4(11)			57(22)
8146.7(3)	0.63(23)	1	54(7)
8183.1(9)			45(15)
8200.2(6)	0.38(14)	(1)	57(13)
8220.6(4)	0.40(10)	(1)	103(14)
8254.2(4)	0.60(20)	1	47(7)
8288.1(16)			21(8)
8347.2(3)	0.70(20)	1	31(7)
8363.5(9)			65(17)
8467.8(5)	0.47(23)	(1)	66(14)
8527.8(8)			39(17)
8568.6(9)			54(24)
8584.0(6)	0.57(24)	1	69(22)
8599.5(6)	0.43(17)	(1)	63(17)
8673.5(5)			26(5)
8796.3(6)			45(10)
8948.8(9)			38(15)
8968.6(6)			22(5)
8987.1(2)	0.76(17)		77(9)
9074.0(5)	0.88(29)	(1)	28(4)
9085.3(4)	0.43(15)	(1)	47(5)
9097.5(3)	0.62(15)	1	54(6)
9148.7(18)			16(5)
9165.0(11)	0.68(28)	1	26(5)
9183.8(13)	0.65(27)	1	24(5)
9197.7(7)	0.64(19)	1	47(7)
9279.0(7)			45(10)
9609.0(4)	0.42(17)	(1)	40(6)

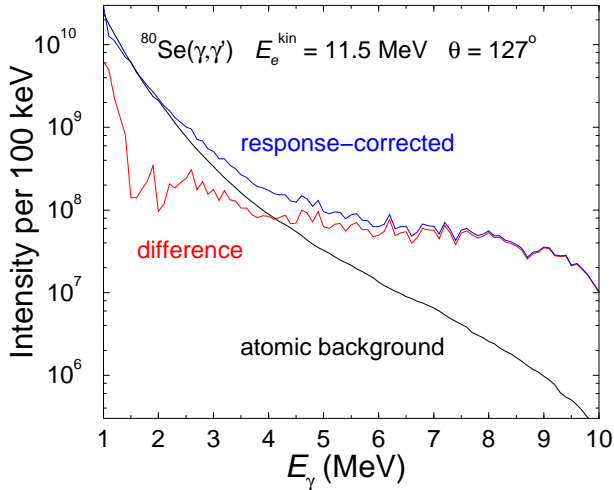[1] Transition energy. The uncertainty of this and the other quanti-

FIG. 3: (Color online) Response-corrected spectrum of the two detectors placed at 127°, simulated spectrum of photons scattered from the target to the detectors by atomic processes, and the difference of the two.

E. Determination of the photoabsorption cross section

For the further analysis, the experimental spectrum was corrected for the detector response and the absolute efficiency as described in Sec. II C, and for the absolute photon flux, background radiation, and atomic processes induced by the impinging photons in the ^{80}Se target.

First, a spectrum of the ambient background adjusted to the intensities of the transitions from ^{40}K and ^{208}Tl decay in the in-beam spectrum was subtracted from the measured spectrum. To correct the spectrum for the detector response, spectra of monoenergetic γ rays were calculated in steps of 10 keV by using the simulation code GEANT4. Starting from the high-energy end of the experimental spectrum, the simulated spectra were subtracted sequentially (spectrum-strip method). The response- and efficiency-corrected spectrum is shown in Fig. 3. The background produced by atomic processes in the ^{80}Se target was obtained from a GEANT4 simulation using the absolute photon flux deduced from the intensities of the transitions in ^{11}B (cf. Fig. 2). The

corresponding background spectrum is also displayed in Fig. 3.

As can be seen in Fig. 3 the spectrum of photons scattered from ^{80}Se contains resolved peaks and a continuum that is remarkably higher than the background caused by atomic scattering processes. This continuum is formed by a large number of non-resolved transitions of small intensities which are a consequence of the high nuclear level density at high energy in connection with the finite detector resolution. The relevant intensity of the photons resonantly scattered from ^{80}Se is obtained from a subtraction of the atomic background from the response-corrected experimental spectrum.

To deduce the correct dipole-strength distribution, inelastic transitions have to be removed from the spectrum and the ground-state transitions have to be corrected for their branching ratios b_0. We applied statistical methods to estimate the intensities of branching transitions to low-lying excited levels and of the branching ratios of the ground-state transitions. These methods were also applied in earlier photon-scattering experiments at γELBE [11, 12, 14–18, 23, 25, 27, 28].

The intensity distribution contains ground-state transitions and, in addition, branching transitions to lower-lying excited states (inelastic transitions) as well as transitions from those states to the ground state (cascade transitions). The different types of transitions cannot be clearly distinguished. However, for the determination of the photoabsorption cross section and the partial widths Γ_0 the intensities of the ground-state transitions are needed. Therefore, contributions of inelastic and cascade transitions have to be subtracted from the spectra. We corrected the intensity distributions by simulating γ-ray cascades from the levels in the whole energy range. The code γDEX [11, 25, 27, 28] was used to do this. γDEX works analogously to the strategy of the code DICEBOX [77] developed for (n, γ) reactions, but in addition includes also the excitation from the ground state. In these simulations, level schemes (nuclear realizations) including states with $J = 0, ..., 5$ were created. We apply the statistical methods also for the low-energy part of the level scheme instead of using experimentally known low-lying levels, because this would require the knowledge of the partial decay widths of all transitions populating these fixed levels. Fluctuations of the partial widths were treated by applying the Porter-Thomas distribution [78].

Level densities were calculated by using the constant-temperature model [79] with the parameters $T = 0.77(4)$ MeV and $E_0 = -0.46(29)$ MeV adjusted to experimental level densities [80]. In the individual nuclear realizations, the values of T and E_0 were varied randomly within a Gaussian distribution with a σ corresponding to the uncertainties given in Ref. [80]. The parity distribution of the level densities was modeled according to the information given in Ref. [81].

The first input for the photon strength function simulations were assumed to be Lorentz-shaped. For the $E1$

ties in the table is given in parentheses in units of the last digit.

[2] Ratio of the intensities measured at angles of 90° and 127°. The expected values for an elastic dipole transition from and to the ground state (spin sequence $0 - 1 - 0$) and for an elastic quadrupole transition (spin sequence $0 - 2 - 0$) are 0.74 and 2.15, respectively.

[3] Spin of the excited state deduced from the given ratio of the intensities measured at angles of 90° and 127° for an assumed ground-state transition.

[4] Energy-integrated scattering cross section deduced from the intensities measured at 127°.

[5] Taken from Ref. [76].

strength a combination of three Lorentz functions (TLO), with parameters as described in Ref. [82], was used with a quadrupole deformation of $\beta_2 = 0.23$ and a triaxiality parameter of $\gamma = 22°$ [83]. The parameters for the $M1$ and $E2$ strengths were taken from global parameterizations of $M1$ spin-flip resonances and $E2$ isoscalar resonances, respectively [84].

Spectra of γ-ray cascades were generated for groups of levels in 100 keV bins. Starting from the high-energy end of the experimental spectrum, which contains ground-state transitions only, the simulated intensities of the ground-state transitions were normalized to the experimental ones in the considered bin. The intensity distribution of the branching transitions was subtracted from the experimental spectrum. Applying this procedure step-by-step for each energy bin moving toward the low-energy end of the spectrum, one obtains the intensity distribution of the ground-state transitions. Simultaneously, the branching ratios b_0^Δ of the ground-state transitions are deduced for each energy bin Δ. In an individual nuclear realization, the branching ratio b_0^Δ is calculated as the ratio of the sum of the intensities of the ground-state transitions from all levels in Δ to the total intensity of all transitions depopulating those levels to any low-lying levels including the ground state [11, 12, 14–18, 23, 25, 27, 28]. By dividing the summed intensities in a bin of the experimental intensity distribution of the ground-state transitions with the corresponding branching ratio, we obtain the absorption cross section in each bin as $\sigma_\gamma^\Delta = \sigma_{\gamma\gamma}^\Delta / b_0^\Delta$ for each nuclear realization. Finally, the absorption cross sections of each bin were obtained by averaging over the values of the nuclear realizations. For the uncertainty of the absorption cross section a 1σ deviation from the mean has been taken.

The simulations were performed iteratively. The strength function obtained from an iteration step was used as the input for the next step. The iteration was stopped when the input strength function and the output strength function were in agreement within their uncertainties. Toward low energy, the uncertainties increase due to the use of the spectrum-strip method and the cross sections do not converge. Therefore, cross sections are not given below excitation energies of 5.5 MeV. In Fig. 4, the input cross sections and the ones obtained from the first and last iteration steps are shown.

III. DISCUSSION

The photoabsorption cross section of ^{80}Se obtained from the experiment just described is shown in Fig. 5, together with cross sections deduced from (γ, n) experiments [62, 85] and with the TLO mentioned in Sec. II E. The cross section deduced from the present analysis continues the (γ, n) cross section toward low energy below $S_n = 9.9$ MeV and fits the (γ, n) cross section around S_n. The cross section shows a structure of three humps at about 7, 8 and 9.5 MeV, respectively. For comparison,
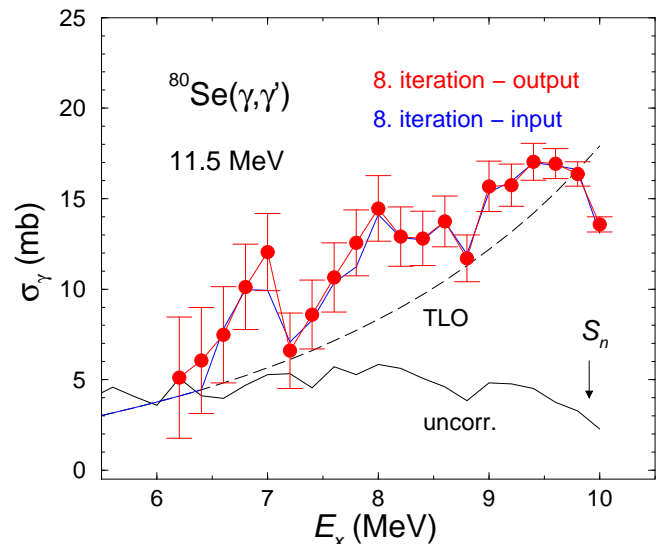

FIG. 4: (Color online) Uncorrected photoabsorption cross section (black solid line), TLO (dahed line), input (blue solid line) and output (red circles with error bars) of the 8. (last) iteration step in the simulation of γ-ray cascades.

the absorption cross section derived for the neighboring isotope ^{78}Se in Ref. [11] displays two humps at about 8 and 10 MeV, respectively, and exceeds the one in ^{80}Se by about 30% in the energy range from about 8 to 10 MeV. In the energy range from about 7 to 9 MeV, the absorption cross section determined for ^{76}Se in Ref. [10] is a factor of 3 to 5 lower than the present one for ^{80}Se. In Ref. [10] there are however no data at energies higher than about 9 MeV, which prevents the data from being compared with the (γ, n) data around $S_n = 11.2$ MeV in ^{76}Se. According to the discussion in Ref. [10], one likely reason for the comparably smaller cross section of ^{76}Se is that intensities of branching transitions to low-lying excited states and strength in the quasicontinuum were not fully taken into account.

In order to evaluate the neutron-capture cross section, an experimental photoabsorption cross section (EPACS) was constructed on the basis of the following components.

i) $0 \leq E_\gamma \leq 6.2$ MeV: The TLO model mentioned in Sec. II E is taken, because there is no experimental data in this energy region.

ii) 6.2 MeV $\leq E_\gamma \leq 10.0$ MeV: The photoabsorption cross section deduced from the present (γ, γ') experiment is used.

iii) $E_\gamma > 10.0$ MeV: The photo-neutron cross section taken from Ref. [85] was used.

The calculations were performed using the code TALYS 1.6 [86]. The results for cross sections and reaction rates obtained using EPACS are compared with results using the implemented standard models for $E1$ strength functions, such as the standard Lorentz model (SLO) [87, 88], the generalized Lorentz model (GLO) [89, 90], and the TLO model. For the nuclear level

density, we used the constant-temperature model [79]. Whereas the SLO overestimates the cross sections in the energy region between 6 and 15 MeV, the GLO and TLO agree well with the EPACS results except for the region of the extra enhancement of strength between about 6 and 10 MeV. Below 6 MeV, all results have still uncertainties because of the lack of experimental data (see Fig. 6). Fig. 7 shows the results for the ^{79}Se(n, γ) cross sections calculated using TALYS with various models for the input γSF. The uncertainty on the cross section due to the choice of the nuclear level density (NLD) model, has been estimated by using various NLD models [91–95] and is shown as a blue band. The enhancement of γSF using EPACS results in about a 55% - 98% larger neutron-capture cross section between 1 keV and 1 MeV, compared to the TLO model. The GLO model, which usually gives a lower neutron-capture cross section than the other models, shows a 49% - 59% lower cross section than that of the TLO model. The reason for this effect can be related to the difference between the γSF of GLO and TLO below 5 MeV. We note that a recent evaluation of the photo-neutron experiment [64] shows smaller neutron-capture cross sections than that resulting from EPACS, because their γSF was determined using experimental data above neutron threshold only.

To investigate the effect of the enhanced strength on the s-process nucleosynthesis, the Maxwellian-averaged neutron-capture cross section (MACS) for ^{79}Se was compared with the value given in the KADoNiS (version 0.3) data base, which corresponds to the one given in Ref. [96]. Tendencies found for the various γSF models used to calculate the MACS are similar to the ones just discussed. In the MACS calculations at $kT = 30$ keV, corresponding to the typical s-process environment, the MACS using EPACS input results in 483 mb with upper and lower limits of 1005 mb and 305 mb, respectively. This result is 1.8 times greater than the recommended value of KADoNiS (263 ± 46 mb, see Fig. 8). Figures 9 and 10 show the ^{79}Se(n, γ) and ^{80}Se(γ, n) reaction rates, respectively.

IV. SUMMARY

The dipole-strength distribution in ^{80}Se up to the neutron-separation energy has been studied in a photon-scattering experiment at the ELBE accelerator using a kinetic electron energy of 11.5 MeV for the purpose of the evaluation of the neutron capture cross sections for ^{79}Se. We identified 180 γ transitions below 9.6 MeV.

The measured γ-ray spectrum was corrected for detector response, and the atomic background was subtracted. The remaining intensity is considered to be from nuclear excitations and are included in the analysis. We performed simulations of statistical γ-ray cascades to estimate intensities of inelastic transitions, and to correct the intensities of the ground-state transitions for their branching ratios.

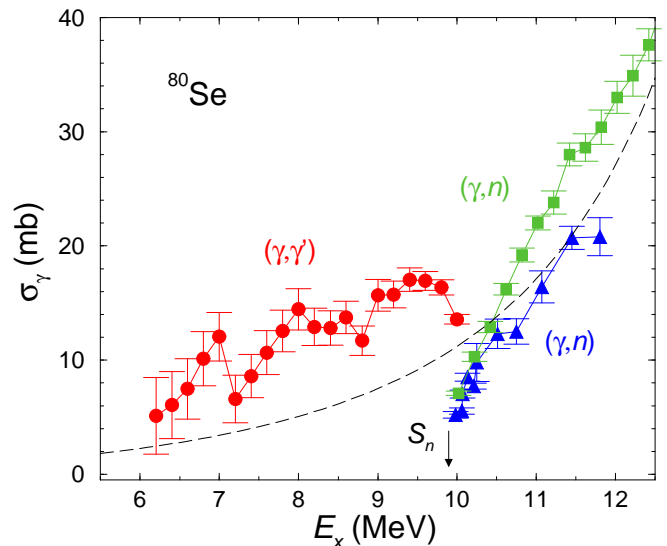The photoabsorption cross section of ^{80}Se below the

FIG. 5: (Color online) Photoabsorption cross sections deduced from the present measurement (red circles) in comparison with (γ, n) data from Ref. [62] (blue triangles) and Ref. [85] (green squares), and with the TLO (black dashed curve).
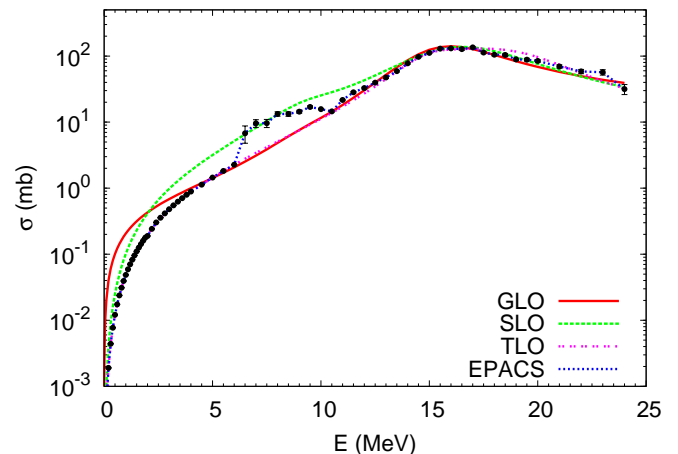

FIG. 6: (Color online) ^{80}Se$(\gamma,$abs$)$ cross sections as a function of γ-ray energy calculated using the code TALYS with various models for the input strength function.

neutron-separation energy obtained from this analysis is combined with the (γ, n) cross section and compared with results of calculations using TALYS. We calculated ^{79}Se(n, γ) cross sections, Maxwellian-averaged cross sections, and reaction rates using the present experimental γSF as an input for TALYS. We found that the observed enhancement in γSF causes a 55% to 98% larger neutron-capture cross section in a neutron energy range between 1 keV and 1 MeV. Below 5 MeV, the lack of experimental data for the γSF in ^{80}Se means that the neutron-capture cross section of ^{79}Se is still uncertain. The present results of Maxwellian-averaged cross section at $kT = 30$
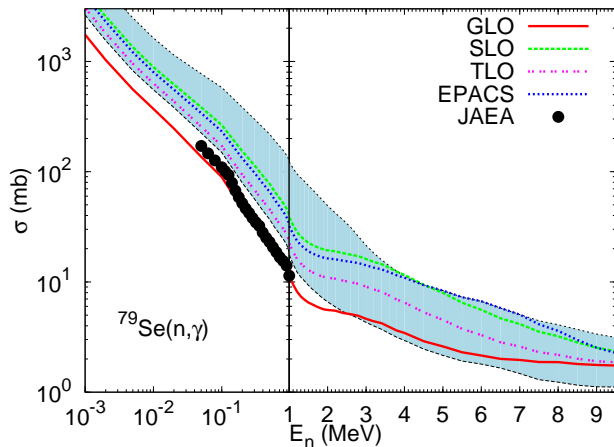
FIG. 7: (Color online) ^{79}Se(n,γ) cross sections as functions of neutron energy calculated using code TALYS with various modes for the input strength function. The uncertainty of the EPACS due to level density model is shown as a blue (gray) band. Recent results of γ strength method obtained from the γSF above neutron threshold [64] are also shown as black points. (see text).
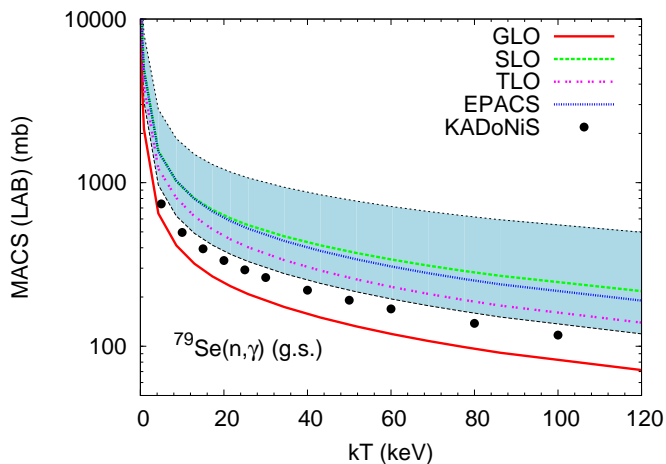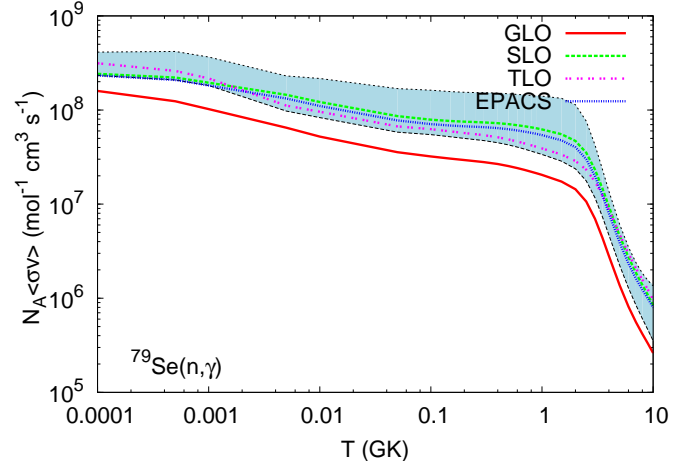
for ^{79}Se may further reduce them.

FIG. 9: (Color online) ^{79}Se(n,γ) reaction rates as a function of temperature, calculated using code TALYS with various models for the input strength function. The uncertainty of the EPACS shown as a blue band results from the use of various nuclear level density models.

FIG. 8: (Color online) ^{79}Se(n,γ) Maxwellian-averaged cross sections calculated using the code TALYS with various models for the input strength function compared with KADoNiS (version 0.3) (black circles). The uncertainty of the EPACS shown as a blue band results from the use of various nuclear level density models.

FIG. 10: (Color online) ^{80}Se(γ,n) reaction rates as a function of temperature, calculated using code TALYS with various models for the input strength function. The uncertainty of the EPACS shown as a blue band results from the use of various nuclear level density models. cross sections.
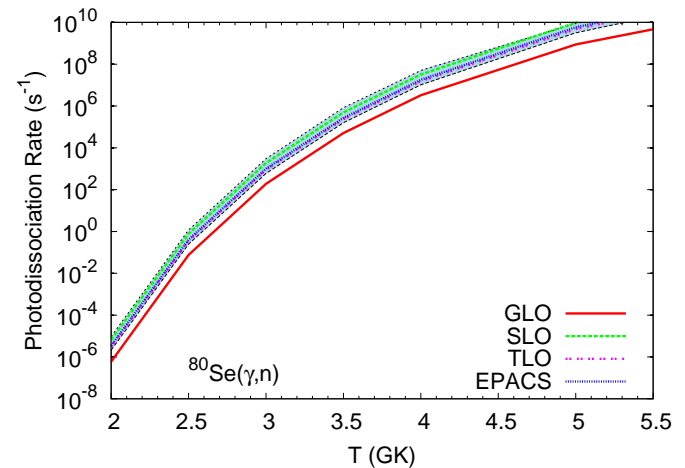
keV is a factor of 1.8 greater than the data of earlier work given in the KADoNiS database. This enhancement of the present result is likely caused by the shape of the experimental γSF below the neutron threshold.

The present calculations have still uncertainties caused by model parameters such as level densities and optical potential parameters. Future direct or indirect methods for the determination of the neutron-capture cross section

[1] Handbook on Photonuclear Data for Applications Cross-sections and Spectra, IAEA-TECDOC-1178 (2000).
[2] E. G. Fuller *et al.*, Nat. Bur. Stand. (U.S.), Spee. Publ. 380 (1973).
[3] N. T. Nyhus *et al.*, Phys. Rev. C**91**, 015808 (2015).
[4] D. M. Filipescu *et al.*, Phys. Rev. C**90**, 064616 (2014).
[5] R. Massarczyk *et al.*, Phys. Rev. C**90**,054310 (2014).
[6] H. Utsunomiya *et al.*, Phys. Rev. C**88**, 015805 (2013).
[7] G. A. Bartholomew, E. D. Earle, A. J. Ferguson, J. W. Knowles, and M. A. Lone, Adv. Nucl. Phys. **7**, 229, (1973).
[8] U. Kneissl, N. Pietralla, and A. Zilges, J. Phys. G **32**, R217 (2006).
[9] D. Savran, T. Aumann, and A. Zilges, Prog. Part. Nucl. Phys. **70**, 210 (2013).
[10] P. M. Goddard *et al.*, Phys. Rev. C **88**, 064308 (2013).
[11] G. Schramm *et al.*, Phys. Rev. C **85**, 014311 (2012).
[12] G. Rusev *et al.*, Phys. Rev. C **77**, 064321 (2008).
[13] G. Rusev *et al.*, Phys. Rev. C **79**, 061302(R) (2009).
[14] R. Schwengner *et al.*, Phys. Rev. C **76**, 034321 (2007).
[15] R. Schwengner *et al.*, Phys. Rev. C **78**, 064314 (2008).
[16] N. Benouaret *et al.*, Phys. Rev. C **79**, 014303 (2009).
[17] G. Rusev *et al.*, Phys. Rev. C **79**, 061302(R) (2009).
[18] R. Schwengner *et al.*, Phys. Rev. C **87**, 024306 (2013).
[19] A. Zilges, S. Volz, M. Babilon, T. Hartmann, P. Mohr, and K. Vogt, Phys. Lett. B **542**, 43 (2002).
[20] P. Adrich *et al.*, Phys. Rev. Lett. **95**, 132501 (2005).
[21] S. Volz, N. Tsoneva, M. Babilon, M. Elvers, J. Hasper, R.-D. Herzberg, H. Lenske, K. Lindenberg, D. Savran, and A. Zilges, Nucl. Phys. **A779**, 1 (2006).
[22] D. Savran, M. Fritzsche, J. Hasper, K. Lindenberg, S. Müller, V. Yu. Ponomarev, K. Sonnabend, and A. Zilges, Phys. Rev. Lett. **100**, 232501 (2008).
[23] A. Makinaga *et al.*, Phys. Rev. C **82**, 024314 (2010).
[24] A. P. Tonchev, S. L. Hammond, J. H. Kelley, E. Kwan, H. Lenske, G. Rusev, W. Tornow, and N. Tsoneva, Phys. Rev. Lett. **104**, 072501 (2010).
[25] R. Massarczyk *et al.*, Phys. Rev. C **86**, 014319 (2012).
[26] J. Isaak *et al.*, Phys. Lett. B **727**, 361 (2013).
[27] R. Massarczyk *et al.*, Phys. Rev. C **87**, 044306 (2013).
[28] R. Massarczyk *et al.*, Phys. Rev. Lett. **112**, 072501 (2014).
[29] A. Makinaga *et al.*, Phys. Rev. C **90**, 044301 (2014).
[30] N. Ryezayeva, T. Hartmann, Y. Kalmykov, H. Lenske, P. von Neumann-Cosel, V. Y. Ponomarev, A. Richter, A. Shevchenko, S. Volz, and J. Wambach, Phys. Rev. Lett. **89**, 272502 (2002).
[31] T. Shizuma, T. Hayakawa, H. Ohgaki, H. Toyokawa, T. Komatsubara, N. Kikuzawa, A. Tamii, and H. Nakada, Phys. Rev. C **78**, 061303(R) (2008).
[32] R. Schwengner *et al.*, Phys. Rev. C **81**, 054315 (2010).
[33] P. A. Seeger, W. A. Fowler, and D. D. Clayton, Astropys. J. Suppl. **11**, 121 (1965).
[34] F. Käppeler, R. Gallino, S. Bisterzo, W. Aoki, Rev. Mod. Phys, Vol. **83** (2011).
[35] H. Beer and R. L. Macklin, Astrophys. J. **339**, 962 (1989).
[36] R. A. Ward, M. J. Newman, and D. D. Clayton, Astrophys. J. Suppl. **31**, 33 (1976).
[37] N. Prantzos, M. Arnould, and K. -P. Arcoragi, Astrophys. J. **315**, 209 (1987).
[38] N. Langer, J. -P. Arcoragi, and M. Arnould, Astron. Astrophys. **210**, 187 (1989).
[39] N. Prantzos, M. Hashimoto, and K. Nomoto, Astron. Astrophys. **234**, 211 (1990).
[40] C. M. Raiteri *et al.*, Astrophys. J. **367**, 228 (1991).
[41] I. Baraffe, M. F. El Eid, and N. Prantzos, Astron. Astrophys. **258**, 357 (1992).
[42] L.-S. The, M. F. El Eid, and B. S. Meyer, Astrophys. J. **533**, 998 (2000).
[43] L.-S. The, M. F. El eid, and B. S. Meyer, Astrophys. J. **655**, 1058 (2007).
[44] C. M. Raiteri *et al.*. Astrophys. J. **419**, 207 (1993).
[45] M. Limongi, O. Straniero, and A. Chieffi, Astrophys. J. Suppl. **129**, 625 (2000).
[46] S. E. Woosley, A. Heger, and T. A. Weaver, Rev. Mod. Phys. **74**, 1015 (2002).
[47] N. Klay and F. Käppeler, Phys. Rev. C **38**, 295 (1988).
[48] H. Beer, G. Walter, and F. Käppeler, Astrophys. J. **389**, 784 (1992).
[49] K. A. Toukan, K. Debus, F. Käppeler, and G. Reffo, Phys. Rev. C **51**, 1540 (1995).
[50] K. Wisshak *et al.*, Phys. Rev. C **52**, 2762 (1995).
[51] R. Raut *et al.*, Phys. Rev. Lett. **111**, 112501 (2013).
[52] R. Reifarth *et al.*, Astrophys. J. **582**, 1251 (2003).
[53] G. Walter, H. Beer, F. Käppeler, and R.-D. Penzhorn, Astron. Astrophys. **155**, 247 (1986).
[54] G. Walter, H. Beer, F. Käppeler, G. Reffo, and F. Fabbri, Astron. Astrophys. **167**, 186 (1986).
[55] F. Käppeler, H. Beer, and K. Wisshak, Rep. Prog. Phys. **52**, 945 (1989).
[56] B. Singh, Nucl. Data Sheets **70**, 437 (1993).
[57] National Cooperative for the Disposal of Radioactive Waste (NAGRA), TECHNICAL REPORT 02-05, ISSN 1015-2636, 2002.
[58] C. Domingo-Pardo *et al.*, CERN-INTC-2014-005, INTC-I-155 (2014).
[59] S. Nakamura *et al.*, J. Nucl. Sci. and Technol. vol. **45**, 116 (2008).
[60] S. Kamada *et al.*, J. Nucl. Sci. and Technol. vol. **47**, 329 (2010).
[61] H. Wang, Symposium on Nuclear Data 2014, http://www.jaea.go.jp/ndd/symposium/2014/.
[62] A. Makinaga *et al.*, Phys. Rev. C **79**, 025801 (2009).
[63] F. Kitatani *et al.*, J. Nucl. Sci. and Technol. **47**, 367 (2010).
[64] F. Kitatani *et al.*, J. Nucl. Sci. and Technol. **53**, **PAGE** (2016).
[65] R. Schwengner *et al.*, Nucl. Instr. Meth. A **555**, 211 (2005).
[66] Y. Schlesinger, H. Szichman, G. Ben-David, and M. Hass, Phys. Rev. C **2**, 2001 (1970).
[67] H. Szichman, Phys. Rev. C **8**, 1429 (1973).
[68] F. Ajzenberg-Selove, Nucl. Phys. **A506**, 1 (1990).
[69] G. Rusev, A. P. Tonchev, R. Schwengner, C. Sun, W. Tornow, and Y. K. Wu, Phys. Rev. C **79**, 047601 (2009).
[70] S. Agostinelli *et al.*, Nucl. Instrum. Methods A **506**, 250 (2003).
[71] E. Trompler, Diploma thesis, Technische Universität Dresden 2009, Report FZD-523 (ISSN 1437-322X), http://www.hzdr.de/publications/013364/13364.pdf
[72] S. Carson *et al.*, Nucl. Instrum. Method A **618**, 190

(2010).

[73] E. Haug, Rad. Phys. Chem. **77**, 207 (2008).

[74] G. Roche, C. Ducos, and J. Proriol, Phys. Rev. A **5**, 2403 (1972).

[75] F. Salvat, J. D. Martinez, R. Mayol, and J. Parellada, Phys. Rev. A **36**, 467 (1987).

[76] B. Singh, Nucl. Data Sheets **105**, 223 (2005).

[77] F. Bečvář, Nucl. Instr. Meth. A **417**, 434 (1998).

[78] C. E. Porter and R. G. Thomas, Phys. Rev. **104**, 483 (1956).

[79] A. Gilbert and A. G. W. Cameron, Can. J. Phys. **43**, 1446(1965).

[80] T. von Egidy and D. Bucurescu, Phys. Rev. C **80**, 054310 (2009).

[81] S. I. Al-Quraishi, S. M. Grimes, T. N. Massey, and D. A. Resler, Phys. Rev. C **67**, 015803 (2003).

[82] A. R. Junghans, G. Rusev, R. Schwengner, A. Wagner, and E. Grosse, Phys. Lett. B **670**, 200 (2008).

[83] J.-P. Delaroche, M. Girod, J. Libert, H. Goutte, S. Hilaire, S. Péru, N. Pillet, and G. F. Bertsch, Phys. Rev. C **81**, 014303 (2010).

[84] R. Capote *et al.*, Nucl. Data Sheets **110**, 3107 (2009).

[85] A. M. Goryachev, G. N. Zalesnyi, and B. A. Tulupov, Izv. Akad. Nauk SSSR, Ser. Fiz. **39**, 134 (1975); Bull. Acad. Sci. USSR, Phys. Ser. **39**, 116 (1975).

[86] A. J. Koning, S. Hilaire, and M. C. Duijvestijn, AIP Conf. Proc. **769**, 1154 (2005).

[87] D. M. Brink, Nucl. Phys. **4**, 215 (1957).

[88] P. Axel, Phys. Rev. **126**, 671 (1962).

[89] S. G. Kadmenskii, V. P. Markushev, and V. I. Furman, Sov. J. Nucl. Phys. **37**, 165(1983).

[90] J. Kopecky and M. Uhl, Phys. Rev. C **41**, 1941(1990).

[91] S. Goriely, F. Tordeur, and J. M. Pearson, Atom. Data Nucl. Data Tables **77**, 311(2001).

[92] W. Dilg, W. Schantl, H. Vonach, and M. Uhl, Nucl. Phys. A **217**, 269(1973).

[93] A. V. Ignatyuk, J. L. Weil, S. Raman, and G. N. Smirenkin, Sov. J. Nucl. Phys. **29**, No4, 450(1979).

[94] A. V. Ignatyunk, J. L. Weil, S. Raman, and S. Kahane, Phys. Rev. Rev. C**42**, 1504(1993).

[95] S. Goriely, S. Hilaire, and A. J. Koning, Phys. Rev. C**78**, 064307(2008).

[96] Z. Y. Bao, H. Beer, F. Käppeler, F. Voss, K. Wisshak, and R. Rauscher, At. Data Nucl. Tables **76**, 70(2000).